Ensemble Monte Carlo characterization of graded $Al_xGa_{1-x}As$ heterojunction barriers

R. Kamoua, J. R. East, and G. I. Haddad
Center for High Frequency Microelectronics, Solid State Electronics Laboratory, Department of Electrical Engineering and Computer Science, University of Michigan, Ann Arbor, Michigan 48109-2122

(Received 16 November 1989; accepted for publication 11 April 1990)

Injection over and through heterojunction barriers is becoming increasingly more important in modern electronic devices. We consider the properties of graded $Al_xGa_{1-x}As$ heterojunction barriers using a self-consistent ensemble Monte Carlo method. In this paper, we consider barriers with two doping levels, 1×10^{15} cm^{-3} and 1×10^{17} cm^{-3}, and two barrier heights, 100 and 265 meV. The 100-meV barrier resulted in small rectification at room temperature whereas the higher barrier exhibited considerable rectification. In both cases the structure with the lower doped barrier has resulted in a smaller current in both forward and reverse regions due to space-charge effects. The energy and momentum distribution functions deviate from a Maxwellian distribution inside the barrier region and in general show two peaks: one is comprised mainly of electrons near equilibrium and the second arises mainly from ballistic electrons. The higher doped structure resulted in a faster electron relaxation toward equilibrium as a function of position because the electric field decreases rapidly in the barrier region.

I. INTRODUCTION

Heterojunctions have been incorporated in many solid-state devices to enhance the transport properties of electrons and holes.[1] The step in conduction band energy introduced when different band-gap semiconductors are placed next to each other provides a powerful tool for modifying the electron distribution function rapidly in time and space. In this study the electron transport and the current density versus voltage (J-V) characteristics of a graded heterojunction will be investigated using a self-consistent ensemble Monte Carlo method. We consider the effect of barrier doping and barrier height on the J-V characteristics. This study provides guidelines for the choice of heterojunction structures that yield the best results for a particular application. One of the applications toward which this study might be helpful is the incorporation of a heterojunction in the cathode of transferred electron devices,[2] although many other applications are possible.

Al-Omar *et al.*[3] have conducted studies of two terminal heterojunction diodes using the ensemble Monte Carlo method. The present study elaborates on the characterization and the properties of the heterojunction injector rather than the diode that incorporates such an injector. Our results correspond to the steady-state solution of the transport across the structure. The simulation time is much longer than the previous work and is terminated only when the variation in the current density as a function of position is smaller than 1%. In addition, we investigate the effect of barrier doping and barrier height on the current density versus voltage characteristics. In Ref. 3, a "graded barrier diode" which is similar to our structure was only characterized at a single barrier height and doping level. We will show that the transport across the barrier and the resulting J-V characteristics are dependent on the barrier doping and height.

The paper is organized as follows. In Sec. II we present a description of the structure and the transport model. In Sec. III we present the simulated current-voltage characteristics for two cases of barrier height and two cases of barrier doping. We also compare qualitatively these curves with the thermionic emission theory and identify the structure that yields J-V characteristics approaching those of a metal-semiconductor Schottky barrier. The electron transport and the evolution of the momentum and energy distribution functions along the barrier are described in Sec. III. Finally in Sec. IV we summarize our results and provide some conclusions.

II. STRUCTURE AND TRANSPORT MODEL

The structures considered in this study are shown in Fig. 1. They consist of a graded AlGaAs region sandwiched between two n^+ contact regions which are doped at 2.0×10^{17} cm^{-3}. The AlGaAs region is n doped at either 1.0×10^{17} cm^{-3} or 1.0×10^{15} cm^{-3}. The thickness of the barrier region (0.1 μm) is chosen so that the transport across

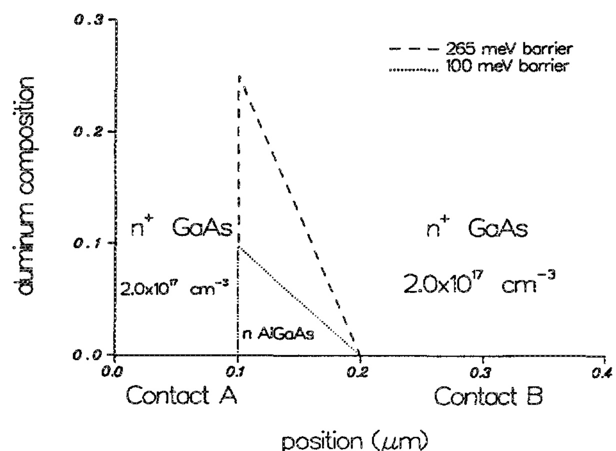

FIG. 1. Aluminum composition and doping profile as a function of position.

 0021-8979/90/151114-09$03.00 © 1990 American Institute of Physics

the structure will be mainly due to thermionic emission processes. Space-charge effects may reduce the potential barrier thickness at electron energies near the maximum barrier height and tunneling may become significant. The effect on the J-V characteristics is equivalent to a reduction of the barrier height. The incorporation of quantum-mechanical tunneling is presently being included in the computer code.

The electron transport model is based on a self-consistent ensemble Monte Carlo method which is an extension of the one-particle Monte Carlo version.[4] We consider a two-valley model consisting of the Γ and the L valleys in the two semiconductor materials.

In order to describe phenomena that are not homogeneous in space, the structure is subdivided into cells of equal length where the different attributes of the electron states are defined and assumed to be constant within each cell. The simulation algorithm consists of monitoring the evolution in real and momentum spaces of an ensemble of electrons. The simulation time is partitioned into time steps each terminated by a call to a Poisson solver in order to update the field. In each time step every electron is submitted to successive free flights terminated by a scattering process which is selected using a random number generator. The scattering mechanisms included are polar optical phonon scattering, acoustic phonon scattering, ionized impurity scattering, intervalley and intravalley phonon scattering, and alloy scattering. Electrons crossing cell boundaries are temporarily stopped at the boundary and then the flight is resumed with the electric field in the new cell. An analogous procedure is followed when it is time to update the electric field and the electron is in the middle of a free flight. In this case the remaining flight time is stored, and the flight is resumed when all other electrons are simulated for one time step and the electric field is updated. To obtain the current density as a function of the applied voltage, the above procedure is repeated at each voltage point until the variation in the current with time and position is less than a certain tolerance.

The electrons are initially distributed in space according to the doping profile using the following mapping between the doping concentration and the actual simulated number of electrons.[5]

$$n_i = \frac{\int_0^L N_d(x)dx}{N_{SE} \times \Delta x} N_{E_i}, \qquad (1)$$

where, n_i = carrier concentration in the ith cell, N_d = doping concentration, N_{SE} = total number of electrons simulated, Δx = space step, N_{E_i} = number of electrons in the ith cell, and L = total length of the structure. When an electron leaves the structure it is injected with a drifted Maxwellian distribution at either of the contacts depending on the sign of the momentum component along the electric field direction. An initial k vector is chosen from a Maxwellian distribution, then the component along the field (z direction) is modified according to the field at the boundaries.

$$kz = kz_{\text{Max}} + \begin{cases} \mu E_A & \text{if } kz_{\text{Max}} > 0 \\ \mu E_B & \text{otherwise,} \end{cases} \qquad (2)$$

where kz_{Max} = momentum along the field obtained from a Maxwellian distribution, kz = momentum along the field with which the electron will be injected, μ = electron mobility in the n^+ regions, and E_A, E_B = magnitudes of the electric field at contact A and contact B respectively. For positive k_z values, the electron is injected from contact A, otherwise it is injected from contact B.

The graded barrier region is modeled by an electric field which is added to the solution of Poisson's equation. The magnitude of this field is given by[6]

$$E_{\text{add}}(x) = \begin{cases} \dfrac{\text{barrier height}}{(\text{electron charge})(\text{barrier width})} \\ \text{for } 0.1\ \mu\text{m} < x < 0.2\ \mu\text{m} \\ 0 \quad \text{otherwise.} \end{cases} \qquad (3)$$

In describing the transport through a compositionally graded region, Al-Omar and Krusius[3] have included the details of the band structure via overlap integrals derived from Γ and L point conduction band wavefunctions for all the scattering mechanisms. They have also taken into account the position dependent effective mass which has been shown to give rise to a quasi-diffusion term in the current density equation.[7] In our model, the scattering rates, the effective mass, and the material parameters correspond to an average aluminum fraction in the barrier. In order to investigate the effects of the above simplifications, we have performed simulations of the barrier structure with position-dependent scattering rates and material parameters and an additional component due to the change in the effective mass was added to the equation of motion. We found that this additional force is opposite to the electric field when the structure is reverse biased and along the field when it is forward biased. This resulted in smaller currents in the reverse bias regions and larger currents in the forward bias regions compared with the results in this paper. The larger the ratio of the average energy to the average electric field, the bigger the difference in the current obtained. The maximum change in the current is about 10% in the reverse bias region and 20% in the forward bias region.

Now we consider the left and right edges of the AlGaAs region, for electrons that cross the right edge we change the scattering rates and the material parameters to correspond to the material to which the electron has crossed into. At the left edge, the electrons are allowed to cross from GaAs to AlGaAs if their energy in the z direction is higher than the band discontinuity energy step ΔE_c. Their energy is then reduced by an amount equivalent to ΔE_c. Electrons that do not meet this condition are reflected back elastically. Electrons crossing the left edge from the AlGaAs region to the GaAs region are always allowed to do so and their energy is increased by ΔE_c. Transfer between a given valley in GaAs (or AlGaAs) and a different valley in AlGaAs (GaAs) at the abrupt interface is not allowed. This is referred to as the "inhibit case"[8] and the restriction is based on the finding that the transmission probability is much smaller in this case than the one corresponding to a similar valley transfer.[9]

The above treatment of the transport across the abrupt interface is equivalent to assuming a classical behavior for electrons impinging on a potential barrier. Quantum-mechanical behavior can be easily incorporated by having an

additional scattering mechanism for electrons that reach the abrupt interface. The probability of this scattering is described by a transmission or a reflection coefficient which can be obtained analytically using for example the WKB method or the tight binding approximation. Glisson *et al.*[10] have compared the classical and the quantum mechanical transmission models when used in describing the transport across a GaAs-$Al_xGa_{1-x}As$ heterostructure. Within the statistical error of the simulation no substantial differences in the results were observed between the two models if the quantum-mechanical transmission coefficient described by Wu and Yand[11] is used.

The space step is 0.005 μm which is less than the Debye length for the doping levels in our structure. The time step to update the electric field is 5×10^{-15} s. The number of electrons simulated is 20 000. Most of the material parameters are taken from Adachi's review article.[12]

III. *J-V* CHARACTERISTICS

In this section we present the *J-V* characteristics of the structure shown in Fig. 1 as obtained from the ensemble Monte Carlo simulation. We consider two barrier heights: the first has a maximum aluminum composition of 0.0975 which corresponds to a barrier height of 100 meV; the second barrier has a maximum aluminum composition of 0.25 which corresponds to a barrier height of 265 meV. In each case we consider two barrier doping levels (10^{15} cm^{-3} and 10^{17} cm^{-3}). The following abbreviations are employed throughout this paper: LDLB = low-doped low barrier (100-meV barrier doped at 10^{15} cm^{-3}), LDHB = low-doped high barrier (265-meV barrier doped at 10^{15} cm^{-3}), HDLB = high-doped low barrier (100-meV barrier doped at 10^{17} cm^{-3}), and HDHB = high-doped high barrier (265-meV barrier doped at 10^{17} cm^{-3}). By analogy with a metal-semiconductor Schottky barrier,[13] we adopt the convention that forward bias corresponds to contact *A* at a higher potential than contact *B*. The opposite case corresponds to a reverse bias configuration.

The current density at a given time and position along the structure is evaluated by keeping track of the number of electrons that cross each cell boundary and the direction of the crossing. In mathematical notation the current density may be expressed as

$$J(x,t) = q\left(\sum_{i=1}^{N_{SE}}\sum_{j=0}^{NC_{i,t}} P_{i,j}(x)\right)\frac{1}{(t-t_0)}\frac{\int_0^L N_d(x)dx}{N_{SE}}, \quad (4)$$

where $J(x,t)$ = current density at time t and position x, t_0 = starting time for the counting process, $NC_{i,t}$ = number of times the *i*th electron has crossed position x in the period $[t_0,t]$, and $P_{i,j}(x)$ = the direction of the *j*th crossing of position x by the *i*th electron and is defined as

$$P_{i,j}(x) = \begin{cases} -1 & \text{if the } j\text{th crossing of position } x \text{ by the } i\text{th electron is from left to right,} \\ 1 & \text{if the } j\text{th crossing of position } x \text{ by the } i\text{th electron is from right to left,} \\ 0 & \text{if } j=0. \end{cases} \quad (5)$$

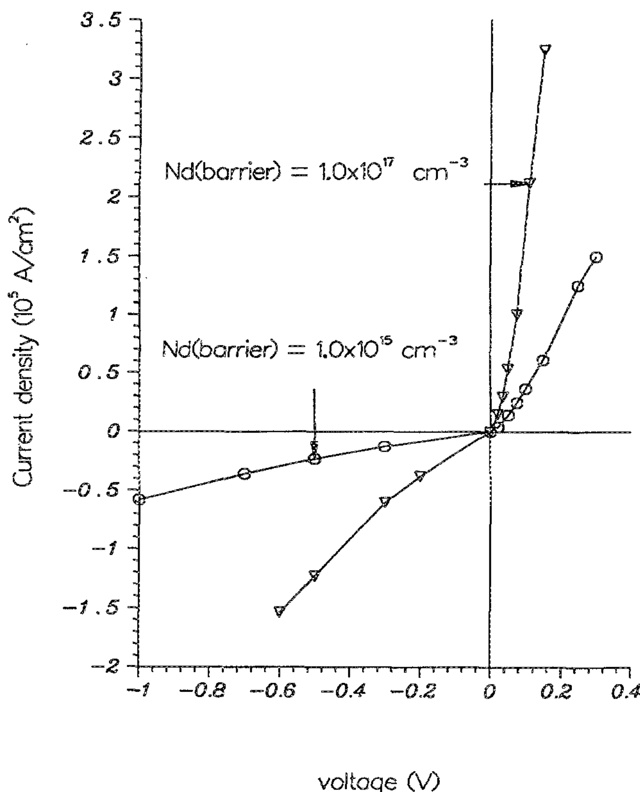

FIG. 2. Current density as a function of the applied voltage for the 100-meV barrier structure.

A. 100-meV barrier structure

We first examine the case where the barrier doping is varied while the barrier height is kept constant at 100 meV. Figure 2 shows the current density as a function of the applied voltage at the two doping levels. We observe that the LDLB structure exhibits a lower current density than the HDLB structure in both forward and reverse directions. In the forward direction, the current in the HDLB structure increases rapidly whereas the LDLB structure exhibits a smaller current and a higher turn on voltage. This behavior can be explained by considering the space-charge effects. At forward voltages below the barrier height, the charge distributions in the LDLB and the HDLB structures are different. The LDLB structure has a depletion region in contact *A* near the abrupt interface and an accumulation region in the barrier followed by a depletion region near the interface between the barrier and contact *B*. On the other hand, the HDLB structure has a depletion region inside the AlGaAs barrier near the abrupt interface, followed by an accumulation then a depletion region inside Contact *B*. Moreover the size of the depletion region at the interface between contact *B* and the barrier is much larger in the LDLB structure than the corresponding depletion in the HDLB structure. This is due to the larger diffusion of electrons from the contact *B* region into the barrier region in the former structure. This explains why the current in the LDLB structure is smaller than the current in the HDLB structure since a larger deple-

tion region results in a stronger opposition to the flow of electrons from contact B to contact A. These space-charge effects manifest themselves in the potential energy diagram as a higher potential barrier in the AlGaAs region of the LDLB structure. Figure 3(a) compares the potential energy diagram and Fig. 3(b) the change in the equilibrium electron density ($n - N_d$) in the two structures at a forward bias of 0.075 V.

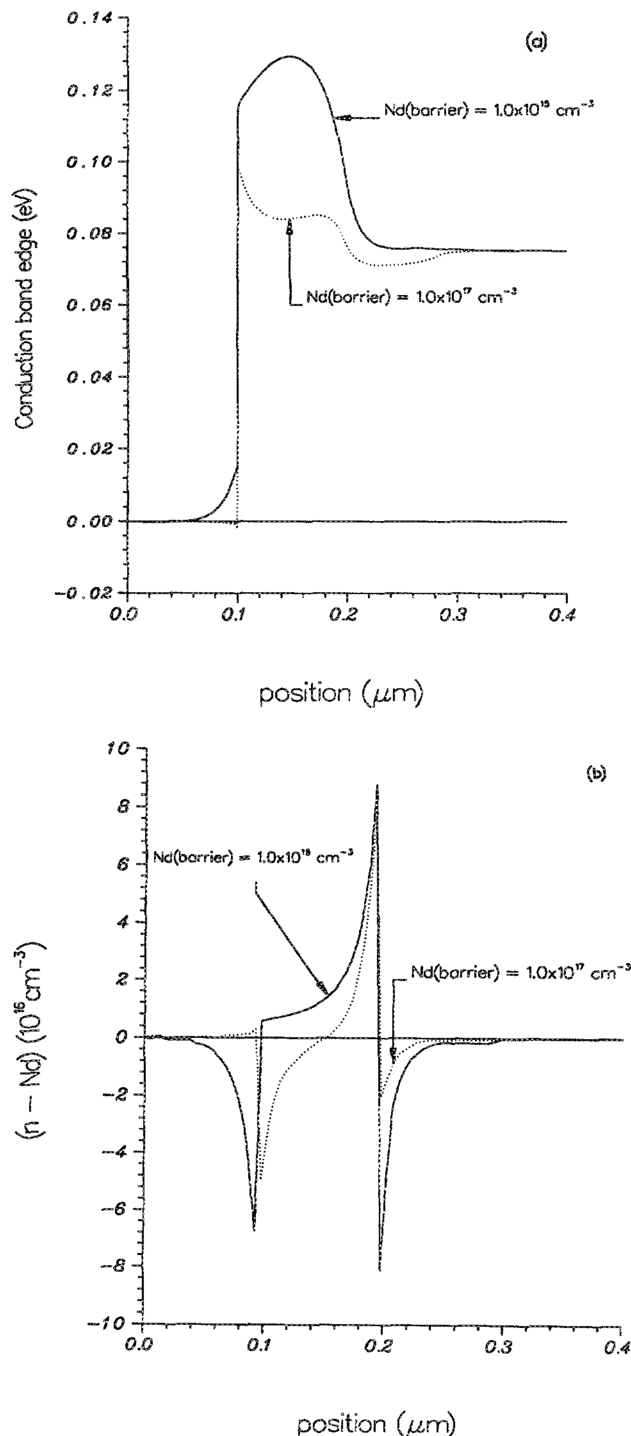

FIG. 3. Comparison of the potential energy diagram (a), and excess electron density (b) between the LDLB and the HDLB structures. The applied forward voltage is 0.075 V in both structures.

In the reverse direction there is a significant current flow in both the HDLB and the LDLB structures and the current increases almost linearly with voltage at large reverse biases. These observations are in agreement qualitatively with the theoretical and experimental work conducted by Chang[14] on Ge-GaAs$_{1-x}$P$_x$ n-n heterojunctions. The increase of the current at reverse biases is due to the voltage drop in the n^+ contact A region which has the effect of increasing the electron energy prior to the abrupt interface. This voltage drop increases as the doping in the barrier is made higher while the doping at the contacts is kept constant. This explains why the HDLB structure has higher current levels compared to those of the LDLB structure. A metal-semiconductor Schottky junction with a similar barrier height would exhibit much more rectification as a result of the much smaller voltage drop in the metal region.

B. 265-meV barrier structure

Increasing the barrier height to 265-meV results in the J-V characteristics shown in Fig. 4. In the forward direction we observe a behavior similar to the 100-meV barrier case except that the turn on voltage is larger, as expected. However, in the reverse direction the current is very small for voltages up to -1 V. The current is probably underestimated because field emission (tunneling) and image force lowering of the barrier are neglected. The turn on voltage is shifted toward higher values by a much larger amount in the reverse direction compared to the forward direction because of the asymmetry of the structure. In the forward direction

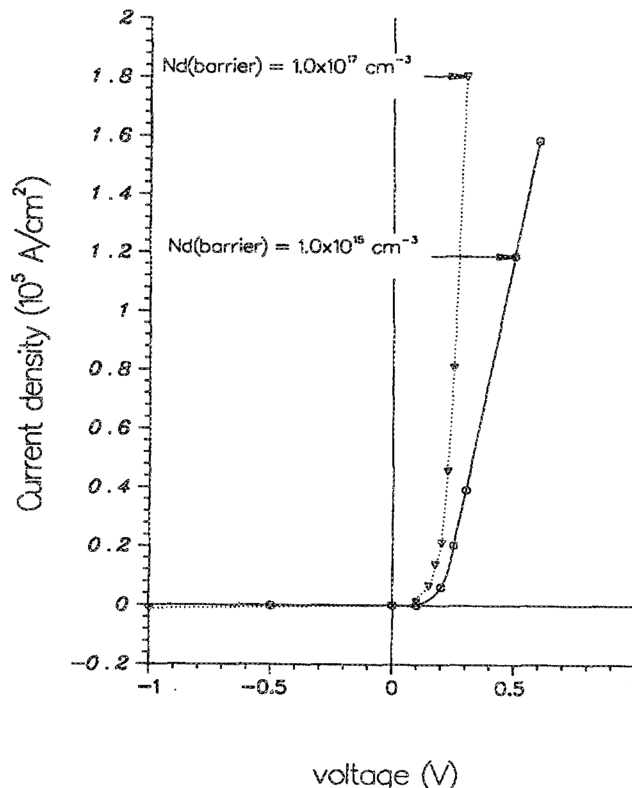

FIG. 4. Current density as a function of the applied voltage for the 265-meV barrier structure.

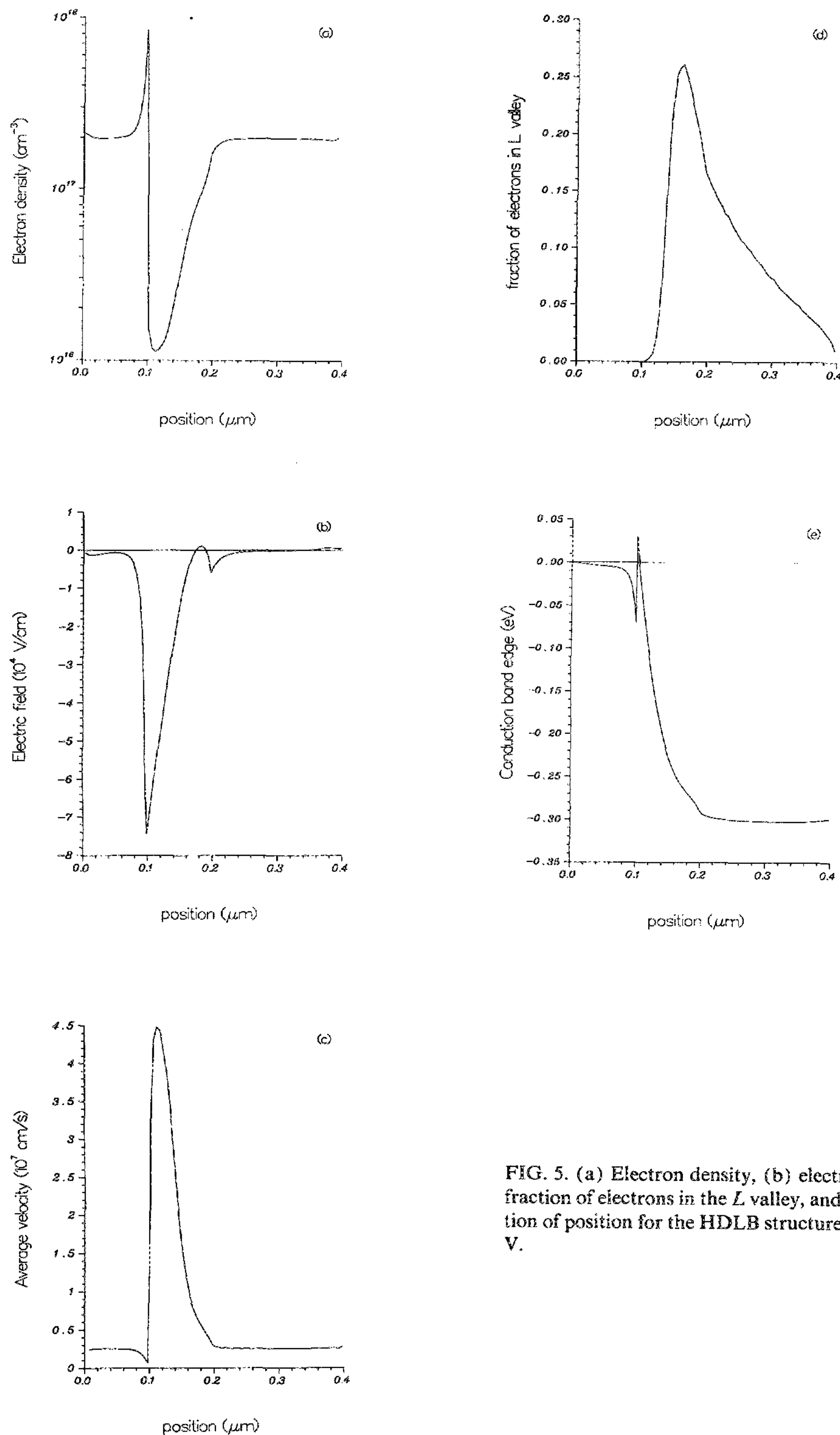

FIG. 5. (a) Electron density, (b) electric field, (c), average velocity, (d) fraction of electrons in the L valley, and (e) the potential energy as a function of position for the HDLB structure. The applied reverse voltage is 0.3 V.

the injection of electrons is from contact B to contact A. The energy band edge of contact B and the graded section of the barrier are shifted upwards resulting in a reduction of the effective barrier height. However, in the reverse direction the electron injection is from contact A to contact B and the electrons see an energy barrier that changes slowly with voltage due to the abrupt barrier interface between contact A and the AlGaAs region. The asymmetry in our structure refers to the energy-band diagram, however asymmetry of the J-V characteristics can also be obtained when the contact regions have different doping levels.[15]

In summary, the J-V characteristics of graded heterojunction barriers can be modified by changing the barrier doping, the contact region doping, the barrier height, and the barrier thickness. These characteristics are close to those of a metal-semiconductor Schottky barrier when the contact

to barrier doping ratio is small and the barrier height is large. The small contact-to-barrier doping ratio results in a higher space-charge limited saturation current in the forward direction, hence the exponential behavior is observed up to higher voltages. The high barrier results in a large increase in the reverse turn on voltage and consequently more rectification.

IV. TRANSPORT PROPERTIES ACROSS GRADED HETEROJUNCTIONS

In this section we describe in more detail the electron transport in the different structures and the effect of barrier doping. We consider the low barrier structure biased in the reverse region where the electric field reaches much higher values than in the forward direction.

A. Transport in the HDLB structure

Figure 5 shows the electron density, electric field, average velocity, fraction of electrons in L valley, and the potential energy as a function of position with an applied reverse voltage of 0.3 V. There is a narrow accumulation region just before the left heterointerface and a depletion region in most of the barrier region [Fig. 5(a)]. As a result, the electric field peaks at the left interface and decreases rapidly in the depletion region [Fig. 5(b)]. The average velocity of the two valleys decreases prior to the abrupt interface due to electron reflections, then overshoots to 4.5×10^7 cm/s within $0.02\,\mu$m inside the barrier [Fig. 5(c)]. The rapid decrease in the average velocity as a function of distance is the result of scattering effects and the transfer of electrons to the L valley. Figure 5(d) shows the fraction of electrons in the L valley which has a peak of 25% halfway into the barrier. The voltage drop in the GaAs region prior to the barrier represents 24% of the total applied voltage [Fig. 5(e)].

We now consider the evolution of the electron energy and momentum distributions across the barrier. The average energy distribution function at four different positions is shown in Fig. 6(a). At $0.105\,\mu$m from the left contact (or $0.005\,\mu$m from the left edge of the barrier), the distribution function is approximately drifted Maxwellian as a result of the electron heating by the large electric field. At $0.14\,\mu$m, the distribution function develops two peaks of approximately equal amplitudes. The first peak centered around 15 meV corresponds to electrons that are being scattered effectively and their energy is relaxing toward thermal equilibrium. The second peak centered around 160 meV corresponds to electrons that have experienced few or no inelastic scatterings and little randomizing of the momentum in the direction of the electric field. These electrons are the so-called ballistic electrons. At $0.18\,\mu$m, the second peak becomes much smaller than the first peak which implies that the energy and momentum scattering events have reduced the number of ballistic electrons and most of the electrons are returning to thermal equilibrium. Finally at $0.22\,\mu$m (or $0.02\,\mu$m after the right edge of the barrier), the distribution function is again approximately Maxwellian. This rapid energy relaxation toward equilibrium in space is due to the fast decrease of the electric field.

A similar plot of the energy distribution function of the

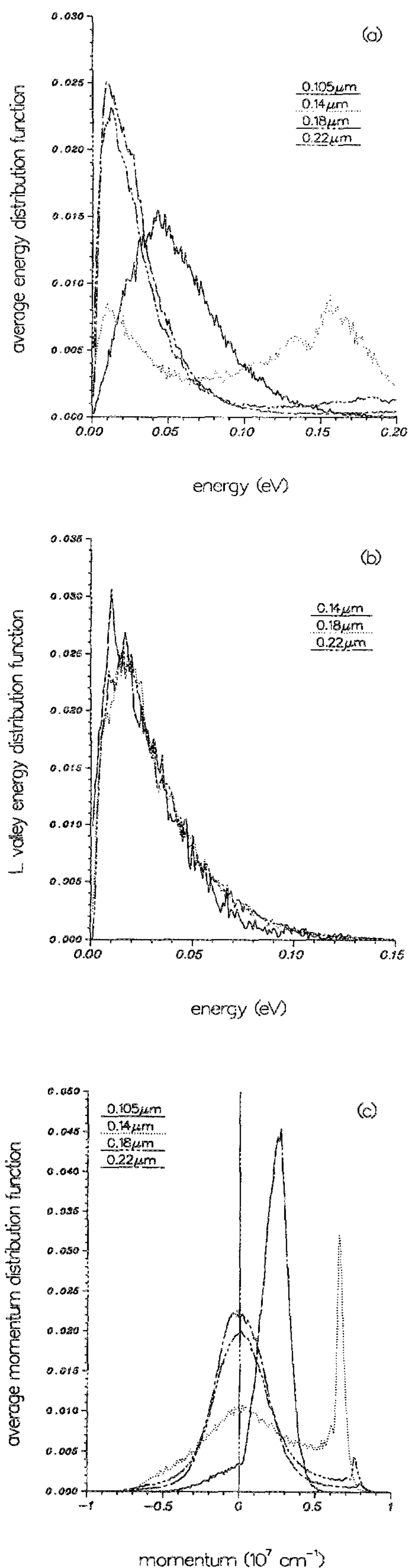

FIG. 6. Energy and momentum distribution functions in the HDLB structure at four barrier positions; (a) corresponds to the average energy distribution in the two valleys, and (b) corresponds to the L valley energy distribution function; (c) corresponds to the average momentum distribution function along the field.

electrons residing in the L valley is shown in Fig. 6(b). The distribution at the first position near the abrupt interface is not shown because there are very few electrons in the L valley. We observe that the distribution function remains Maxwellian at the three different positions which is a result of the higher effective mass and the larger scattering rates in the L valley. This shows that the ballistic electrons are Γ valley electrons because once they scatter to the L valley they experience momentum randomization.

The average momentum distribution function along the electric field is shown in Fig. 6(c) at the same four positions. At $0.14\,\mu m$, we observe a narrow and large peak in the distribution function. Simple calculations show that the average momentum of this peak corresponds to a momentum gained by an average electric field over $0.04\,\mu m$ assuming no collisions which justifies describing these electrons as ballistic.

B. Transport in the LDLB structure

We now consider the LDLB structure and show in Fig. 7 plots similar to Fig. 5, however the applied reverse voltage is now 0.6 V which yields close to half the current density level compared with the previous structure. The accumulation of electrons prior to the interface is smaller than in the

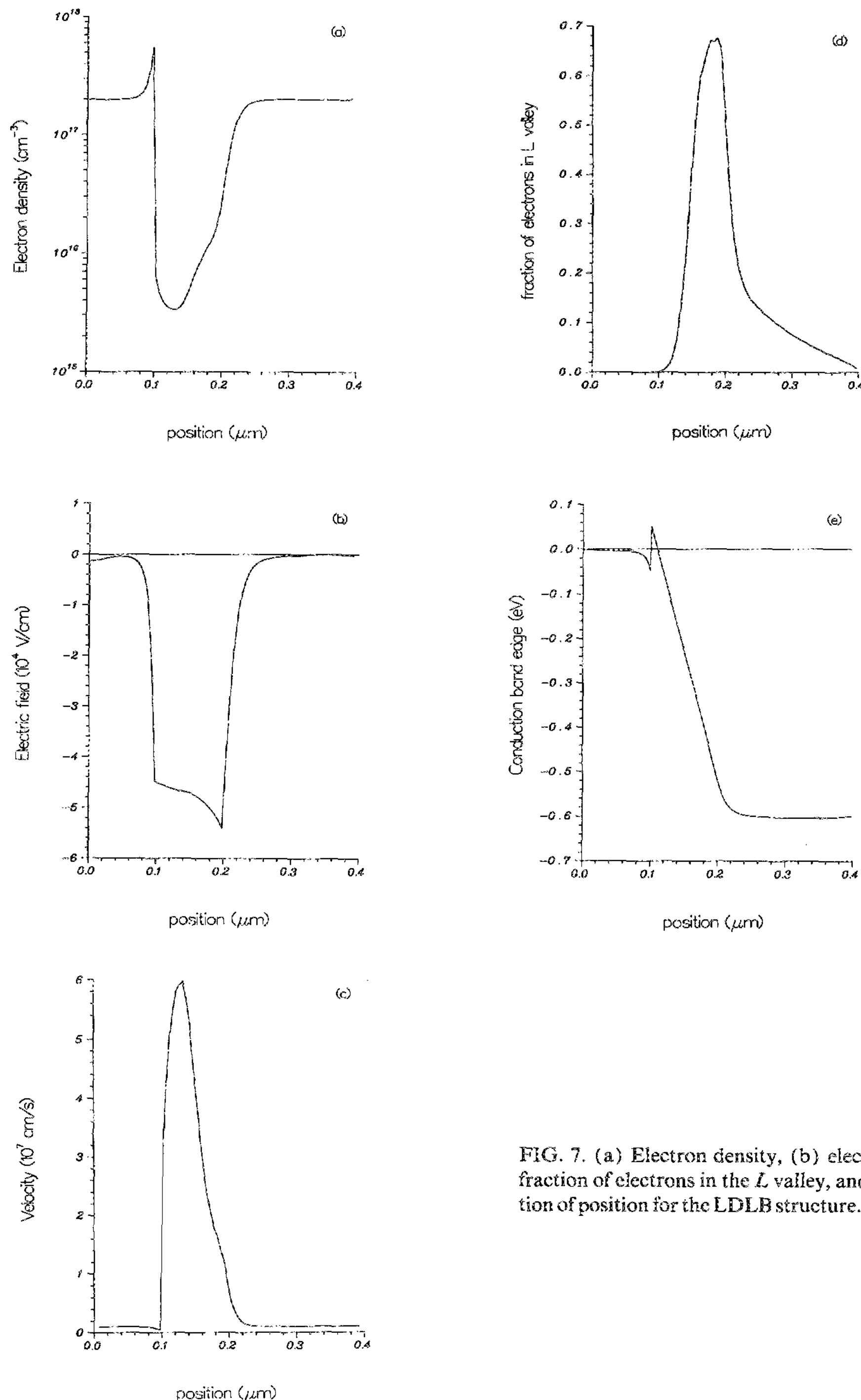

FIG. 7. (a) Electron density, (b) electric field, (c) average velocity, (d) fraction of electrons in the L valley, and (e) the potential energy as a function of position for the LDLB structure. The applied reverse voltage is 0.6 V.

HDLB structure, however there is now an accumulation of electrons in the barrier region [Fig. 7(a)]. As a result, the electric field peaks at the end of the AlGaAs region [Fig. 7(b)]. Although the maximum electric field is lower in this structure, the peak velocity is higher (6.0×10^7 cm/s) as shown in Fig. 7(c) because the electric field remains large for a longer distance inside the AlGaAs region. The fraction of electrons in the L valley reaches values close to 70% [Fig. 7(d)]. The voltage drop in the n^+ contact A region represents 8.5% of the total applied voltage compared with 24% in the HDLB structure [Fig. 7(e)]. As discussed in Sec. III, the smaller voltage drop in contact A results in a lower current density in the LDLB structure for the same applied voltage.

The evolution of the energy and momentum distribution functions are shown in Figs. 8(a) and 8(b) respectively. Comparing the distribution at 0.04 μm into the barrier (curve labeled 0.14 μm) between the LDLB and HDLB structures, we observe that in the LDLB structure the second peak has an amplitude almost three times the first peak whereas in the HDLB structure the two peaks have similar probability amplitudes. We also observe a slower energy relaxation toward equilibrium as a function of position. These differences between the two structures are due to the electric field profile in the barrier region. In the HDLB structure the field is maximum at the left interface and decreases rapidly in the barrier region whereas in the LDLB structure the electric field peaks at the end of the barrier region which results in electrons being hot for a longer distance.

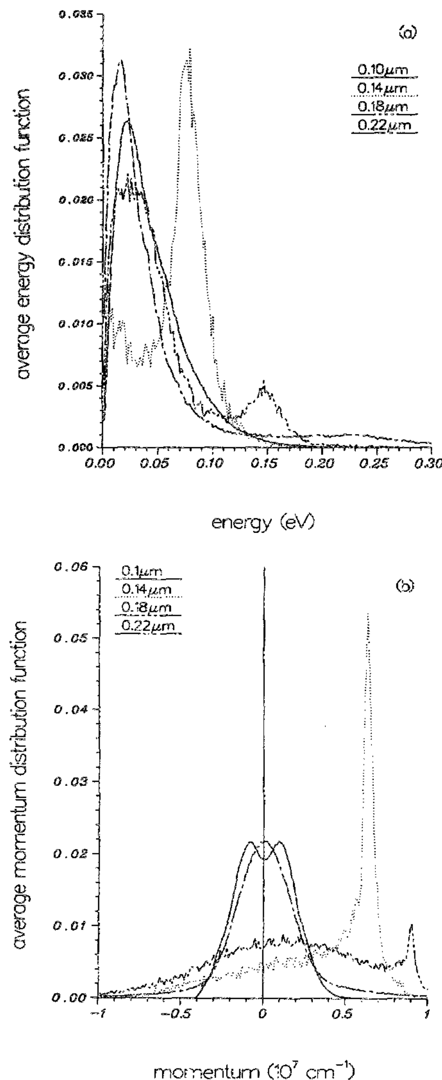

FIG. 8. Energy and momentum distribution functions in the LDLB structure at four barrier positions and a reverse bias of 0.6 V; (a) corresponds to the average energy distribution in the two valleys and (b) corresponds to the average momentum distribution function along the field.

In Ref. 3, the ballistic peak in the momentum distribution function 25 nm downstream from the heterojunction is approximately equal to the peak at zero momentum for a forward-biased injector at 300 K. From the results of the LDLB structure [Fig. 8(b)], we observe that when the injector is reverse biased, the ballistic peak 40 nm downstream is much larger than the peak at zero momentum. This enhancement in the ballistic peak is due to the larger electric field in the reverse biased structure compared with a forward biased structure. In Ref. 3, the electric field downstream from the heterojunction is initially opposing the movement of electrons as can be seen from the conduction-band edge.

It has been suggested that a heterojunction placed in the cathode region of a transferred electron device would decrease the inactive region that is necessary for electrons to start transferring to upper valleys efficiently. The ballistic launcher[3] has resulted in a small increase of the fraction of electrons in the L valley compared with a structure without a launcher. From our results, the fraction of electrons in the L valley reached values close to 70% in the LDLB structure when reverse biased even though the barrier height is 100 meV compared to more than 200 meV in Ref. 3. This suggests that the energy gained by the electrons comes mainly from the large electric field rather than converting the band discontinuity to kinetic energy.

V. CONCLUSIONS

The J-V characteristics of graded GaAs-AlGaAs-GaAs structures have been explored using a self-consistent ensemble Monte Carlo method. Two barrier heights, 100 and 265 meV and two barrier doping levels, 1.0×10^{15} and 1.0×10^{17} cm^{-3} were considered. The lower barrier structure has shown little rectification at room temperature at both doping levels. Space-charge effects resulted in an accumulation in the barrier region when doped at 1.0×10^{15} cm^{-3} and a depletion region near the abrupt interface when doped at 1.0×10^{17} cm^{-3}. The accumulation region persisted even at large reverse voltages. In the forward direction, the lower doped barrier structure has shown a deviation from the exponential behavior occurring at lower voltages compared with the high doped structure.

When the barrier height is increased to 265 meV, the turn on voltage in the reverse direction is increased much more than the turn on voltage in the forward direction. This is related to the asymmetry of the energy band in the structure and particularly the abrupt heterojunction interface. Significant rectification is observed at room temperature for both barrier doping levels.

Investigations of the energy and momentum distribution functions along the barrier have shown that the assump-

tion of drifted Maxwellian distribution used in energy-momentum models is not justified for Γ valley electrons. This non-Maxwellian behavior is stronger when the heterojunction barrier is reverse biased. The energy-momentum models based on the assumption that the distribution function is drifted Maxwellian[16] may be inadequate to describe the transport across heterojunctions. An alternative to this deficiency is to couple a more accurate model (such as the ensemble Monte Carlo) with the energy momentum. This is presently being carried out.

ACKNOWLEDGMENTS

This work was supported by the Center for Space Terahertz Technology under Contract No. NAGW-1334 and U.S. Army Research Office under the URI Program, Contract No. DAAL03-87-K-0007.

[1]H. Kroemer, Proc. IRE **45**, 1535 (1957).
[2]N. R. Couch, H. Spooner, P. H. Beton, M. J. Kelly, M. E. Lee, P. K. Rees, and T. M. Kerr, IEEE Electron Device Lett. **10**, 288 (1989).
[3]A. Al-Omar and J. P. Krusius, J. Appl. Phys. **62**, 3825 (1987).
[4]W. Fawcett, A. D. Boardman, and S. Swain, J. Phys. Chem. **31**, 1963 (1970).
[5]J. Zimmermann and E. Constant, Solid-State Electron. **23**, 915 (1980).
[6]M. R. Friscourt, P. A. Rolland, and M. Pernisek, IEEE Electron Device Lett. **EDL-6**, 497 (1985).
[7]K. Tomizawa, Y. Awano, and N. Hashizume, IEEE Electron Device Lett. **EDL-5**, 362 (1984).
[8]Y. Cho, R. Sakamoto, and M. Inoue, Solid-State Electron. **31**, 325 (1988).
[9]G. C. Osbourn and D. L. Smith, J. Vac. Sci. Technol. **16**, (1979).
[10]T. H. Glisson, J. R. Hauser, M. A. Littlejohn, K. Hess, B. G. Streetman, and H. Shichijo, J. Appl. Phys. **51**, 5445 (1980).
[11]C. M. Wu and E. S. Yang, Solid-State Electron. **22**, 241 (1979).
[12]Sadao Adachi, J. Appl. Phys. **58**, R1 (1985).
[13]S. M. Sze, *Physics of Semiconductor Devices* (Wiley, New York, 1969).
[14]L. L. Chang, Solid-State Electron. **8**, 721 (1965).
[15]T. W. Hickmott, P. M. Solomon, R. Fisher, H. Morkoç, J. Appl. Phys. **57**, 2844 (1985).
[16]K. Blotekjaer, IEEE Trans. Electron Devices **ED-17**, 38 (1970).